mathematics

MDPI

Article

Dual Solutions of Unsteady Mixed Convection Hybrid Nanofluid Flow Past a Vertical Riga Plate with Radiation Effect

Rusya Iryanti Yahaya [1], Norihan Md Arifin [1,2], Ioan Pop [3,4,*], Fadzilah Md Ali [1,2] and Siti Suzilliana Putri Mohamed Isa [1,5]

[1] Institute for Mathematical Research, Universiti Putra Malaysia, Serdang 43400, Malaysia
[2] Department of Mathematics, Universiti Putra Malaysia, Serdang 43400, Malaysia
[3] Department of Mathematics, Babeş-Bolyai University, R-400084 Cluj-Napoca, Romania
[4] Academy of Romanian Scientists, 050044 Bucharest, Romania
[5] Centre of Foundation Studies For Agricultural Science, Universiti Putra Malaysia, Serdang 43400, Malaysia
* Correspondence: popm.ioan@yahoo.co.uk

Abstract: A mathematical model for the unsteady, two-dimensional mixed convection stagnation point flow over a Riga plate is presented in this study. Convective boundary conditions, time-dependent derivatives, mixed convection, radiation effects, and the Grinberg term were all incorporated into the formulation of the governing equations and boundary conditions. By incorporating similarity transformations, ordinary differential (similarity) equations (ODEs) are derived from the partial differential equations (PDEs) of the flow model. The boundary value problem of the fourth-order accuracy code (bvp4c) was implemented in MATLAB (2017b, The MathWorks, Inc., Natick, MA. USA, 2017) to solve the mathematical model numerically. Due to the plate's shrinking motion, two (dual) solutions are possible (first and second solutions). Based on the stability analysis, it was found that the first solution is stable and physically realizable in practice, while the second solution is not stable and not physically realizable in practice. It was found that the increase in the mixed convection parameter, modified Hartmann number, and unsteadiness parameter improved the hybrid nanofluid's temperature profile. In addition, increasing the unsteadiness parameter decreased the velocity profile and the skin friction coefficient. Thus, the numerical results suggested that the augmentation of the modified Hartmann number, mixed convection parameter, and unsteadiness parameter can enhance the heat transfer performance in this flow model. This study offers valuable insight into fundamental transport phenomena such as the transmission of momentum, heat, or mass. Hence, it provides valuable information on the gradients of essential factors to control the boundary layer flow pattern.

Keywords: Riga plate; hybrid nanofluid; mixed convection; radiation; convective boundary condition

MSC: 76W05; 76D10; 80A21; 35Q35

Citation: Yahaya, R.I.; Arifin, N.M.; Pop, I.; Ali, F.M.; Isa, S.S.P.M. Dual Solutions of Unsteady Mixed Convection Hybrid Nanofluid Flow Past a Vertical Riga Plate with Radiation Effect. *Mathematics* **2023**, *11*, 215. https://doi.org/10.3390/math11010215

Academic Editor: Lihua Wang

Received: 28 November 2022
Revised: 10 December 2022
Accepted: 29 December 2022
Published: 1 January 2023

1. Introduction

The dispersion of at least two different nanoparticles in a conventional heat transfer fluid produces a hybrid nanofluid. This fluid is manufactured to provide a better heat transfer fluid with a higher thermal conductivity than mono-nanofluids and regular fluids (e.g., water, organic liquids, engine oil, and polymeric solutions). Therefore, the hybrid nanofluid can be employed in a wide range of areas, such as electronic cooling, heat exchangers, military equipment, automotive, solar collectors, and refrigeration systems, in place of mono-nanofluids and conventional fluids [1,2]. In addition, hybrid nanofluids can also be used to enhance the heat transfer performance of cold storage and solar thermal energy storage systems (see Shao et al. [3]; Dubal et al. [4]; Vaka et al. [5]; Selimefendigila et al. [6]; Gao et al. [7]; Maleki et al. [8]; and Alrowaili et al. [9]). Turcu et al. [10], Jana et al. [11], and Suresh et al. [12] were among the first researchers to do experimental

research on the development of hybrid nanofluids. Other researchers then evaluated the synthesis of hybrid nanofluids and their thermophysical properties [13–19]. Despite this, hybrid nanofluids are still in the research and development phase, necessitating considerable research on numerous factors that can affect their heat transfer capability, such as nanoparticle combinations, their mixing ratio, stability, and mechanisms.

The mixture of free and forced convection is referred to as mixed convection. Mixed convection flow is produced when the effects of forced flow in free convection or buoyant force in forced convection become considerable. This flow type becomes prominent when there is a significant temperature difference and/or a low forced flow velocity [20]. The research on mixed convection flow is helpful to numerous industrial applications and technologies, including paper production, steel extrusion, pipeline transport, cooling of metallic plates, nanotechnology, atmospheric boundary layer flows, electronic power supply, and nuclear reactors [21–23]. After the introduction of hybrid nanofluids, several investigations on the mixed convection in hybrid nanofluids were conducted. Different flow regimes and geometries were considered. Khan et al. [24] studied the combined forced and free convection stagnation point flow on a curved surface. Then, Hanif et al. [25] analyzed the unsteady flow past an inverted cone submerged in a porous media. The hybrid nanofluid flow over a horizontal circular cylinder with mixed convection, radiation, magnetic field, and convective boundary condition was then scrutinized by El-Zahar et al. [26]. Patil and Kulkarni [27] and Abbasi et al. [28] conducted more research on hybrid nanofluid flow past a cylinder with mixed convection. In the meantime, Jahan et al. [29] discussed the effects of radiation and viscous dissipation on the mixed convection hybrid nanofluid flow past a thin needle. Then, several other solid boundaries and physical conditions were investigated for the mixed convection flow of hybrid nanofluids, such as flow over a cone with heat radiation and suction/injection analyzed by Patil and Kulkarni [30]. Asghar et al. [31] then investigated the radiation and partial slip effects on the mixed convection flow over a sheet that shrinks exponentially. In addition, Abdelaziz et al. [32], Khan et al. [33], Khan et al. [34], Wahid et al. [23], Gohar et al. [35], Ahmed and Raizah [36], Asghar et al. [37], Wafa and Toufik [38], and Mandal et al. [39] have also undertaken some additional research on hybrid nanofluid flow with mixed convection.

A Riga plate is an electromagnetic actuator composed of alternating electrodes and permanent magnets installed on a flat surface. This revolutionary flow control mechanism, introduced by Gailitis and Lielausis [40], can induce the Lorentz force. In addition to the standard flow control methods (i.e., suction, blowing, and wall motion), electromagnetic body forces can be used to control the flow of an electrically conducting fluid. Classical magnetohydrodynamics (MHD) flow control is applicable to fluids with high specific conductance, such as liquid metals and semiconductor melts [41]. However, fluids with low conductivity (e.g., seawater) require an additional external electric field to achieve the desired flow control (i.e., electromagnetohydrodynamics (EMHD) flow control). Subsequently, the interplay of electric and magnetic fields generates a Lorentz force, which can change the pressure-driven boundary layer flow and stabilize the flow by slowing its growth [42,43]. Thus, it prevents boundary layer separation and turbulent flow.

A Riga plate can introduce the wall-parallel Lorentz force into the boundary layer. Fluid flow past a Riga plate has beneficial applications in mechanical engineering, chemical engineering, civil engineering, and biomedical sciences with the nanofluid flow [44]. Grinberg term, which gives rise to the electromagnetic parameter known as the modified Hartmann number, is also a crucial component for the flow past a Riga plate [45]. This term in the boundary layer momentum equation diminishes exponentially in the direction perpendicular to the plate and is decoupled from the flow [46]. Positive and negative values of the modified Hartmann number represent the assisting and opposing flows, respectively. These flows were studied by Magyari and Pantokratoras [41] with the inclusion of mixed convection. Due to the increase in viscosity caused by the opposite Lorentz force, the fluid velocity in the opposing flow was discovered to decrease. Then, other researchers analyzed the mixed convection nanofluid flow over a Riga plate (see Bhatti et al. [43], Ayub et al. [46],

and Ahmad et al. [47]). The work on the flow over a mixed convection shrinking sheet is a new type of shrinking sheet flow, that is essentially a backward flow, which was discussed by Goldstein [48] and it shows physical phenomena quite distinct than that of the stretching Riga plate.

Following these studies, we investigate the combined forced and free (mixed) convection stagnation point flow of a hybrid Cu–Al_2O_3/H_2O nanofluid across a vertical Riga plate, that was also examined by Khashi'ie et al. [49]. In the previous investigation, numerical computing methods yielded two solutions, but only one was deemed stable. In contrast to the opposing flow, the assisting mixed convection flow generated a higher rate of heat transfer and skin friction coefficient. Additionally, the hybrid nanofluid outperformed the Al_2O_3/H_2O nanofluid and water in terms of skin friction coefficient and heat transfer rate. Then, Zainal et al. [50] broadened this investigation to include the unsteady flow over a stretching/shrinking Riga plate with thermal radiation. This investigation also obtained dual solutions with only one stable solution. When the modified Hartmann number grew, the heat transmission rate increased while the temperature profile of the hybrid nanofluid reduced. However, the heat transmission rate decreased as the thermal radiation parameter increased. Wahid et al. [51] then extended this investigation with a new hybrid nanofluid (i.e., Fe_3O_4–$CoFe_2O_4/H_2O$) and the presence of a velocity slip factor in a steady flow. It was observed that as the velocity slip parameter and modified Hartmann number increased, the skin friction coefficient decreased. In contrast, the heat transmission rate improved due to these parameters. Additional recent and intriguing studies on the mixed convection hybrid nanofluid flow over a Riga plate have also been mentioned (see Ahmad et al. [47]; Alshehri et al. [52]; Khashi'ie et al. [53]; Nadeem et al. [54]; Nayak et al. [55]; Ramzan et al. [56]; Salawu et al. [57]; and Shatnawi et al. [58]).

Based on these earlier investigations by Khashi'ie et al. [49], Zainal et al. [50], and Wahid et al. [51], the current investigation will concentrate on the Cu–Al_2O_3/H_2O hybrid nanofluid's unsteady mixed convection flow across a fixed vertical Riga plate. Thermal radiation and convective boundary conditions will be considered for the heat transfer analysis. The energy equation and boundary condition will each include the terms relevant to these impacts. To the authors' knowledge, this flow problem has not been the subject of any investigations. Therefore, it is interesting to analyze the following:

i. Does this flow problem have multiple solutions?
ii. How does the unsteady flow affect the Nusselt number and skin friction coefficient?
iii. Does the existence of convective boundary conditions improve/diminish the hybrid nanofluid's temperature and velocity distributions?
iv. How do other controlling parameters affect the hybrid nanofluid's temperature and velocity distributions?

Using the bvp4c solver, the regulating equations and associated boundary conditions will be numerically solved. If multiple solutions exist, stability analysis will identify the more reliable solution. The analysis and discussion of the outcomes will then be made based on this reliable solution.

2. Problem Formulation

The hybrid nanofluid's unsteady mixed convection stagnation point flow past a vertical Riga plate is examined in this study. As depicted in Figure 1, $(x,\ y)$ are Cartesian coordinates measured along and normal to the plate, respectively, with the flow occurring in the region $y \geq 0$. The polarity of the magnets on the Riga plate is represented by the letters North (N) and South (S). The Lorentz force is introduced into the system using this formation. Meanwhile, the far-field (hybrid nanofluid) is assumed to have a linear velocity of $u_e(x,t) = a\ x/(1 - c\ t)$, where $(a,\ c)$ are constants with $a > 0$, c shows the unsteadiness of the problem, and t denotes the time. According to Fang et al. [59], if c is positive, the Riga plate shrinks over the time (e.g., contracting), whereas if c is negative, the Riga plate grows over time (e.g., expanding). It is assumed that the convective temperature at the plate surface is $T_f(x,t)$, l is the characteristic length of the Riga plate, T_∞ is the constant

temperature of the base hybrid nanofluid. q_r is the radiation heat flux that can be expressed as [60]:

$$q_r = -\frac{4\,\sigma^*}{3\,k^*}\frac{\partial T^4}{\partial y}. \tag{1}$$

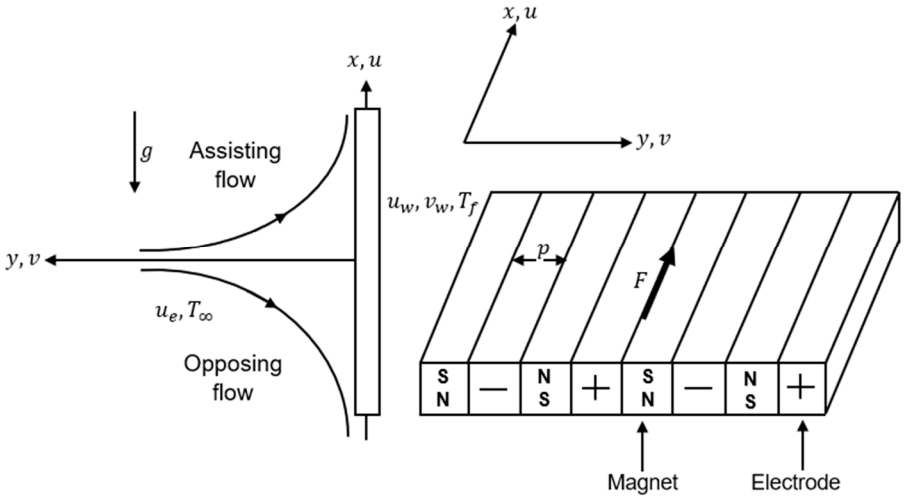

Figure 1. Schematic representation of the flow problem.

The mass, momentum, and energy equations regulating this unsteady flow can be expressed as (see Shatnawi et al. [58]; Devi and Devi [61]):

$$\frac{\partial\,u}{\partial\,x} + \frac{\partial\,v}{\partial\,y} = 0, \tag{2}$$

$$\left.\begin{array}{c} \frac{\partial\,u}{\partial\,t} + u\,\frac{\partial\,u}{\partial\,x} + v\,\frac{\partial\,u}{\partial\,y} = \frac{\partial\,u_e}{\partial\,t} + u_e\frac{\partial\,u_e}{\partial\,x} + \frac{\mu_{hnf}}{\rho_{hnf}}\,\frac{\partial^2 u}{\partial\,y^2} + \\ \frac{\pi\,j_0\,\tilde{M}_0(x,t)}{8\,\rho_{hnf}}e^{\left(-\frac{\pi\,y}{p}\right)} + \beta_{hnf}(T - T_\infty)g \end{array}\right\}, \tag{3}$$

$$\frac{\partial\,T}{\partial\,t} + u\,\frac{\partial\,T}{\partial\,x} + v\,\frac{\partial T}{\partial\,y} = \frac{k_{hnf}}{(\rho\,C_p)_{hnf}}\,\frac{\partial^2 T}{\partial\,y^2} - \frac{1}{(\rho\,C_p)_{hnf}}\frac{\partial\,q_r}{\partial\,y}. \tag{4}$$

By using the Taylor series and ignoring higher-order terms, T^4 can be expanded about T_∞ to obtain $T^4 \approx 4T_\infty^3 T - 3T_\infty^4$, so that Equation (1) becomes:

$$q_r = -\frac{16\,\sigma^* T_\infty^3}{3\,k^*}\frac{\partial T}{\partial y}, \tag{5}$$

and Equation (4) can be written as:

$$\frac{\partial\,T}{\partial\,t} + u\,\frac{\partial\,T}{\partial\,x} + v\,\frac{\partial T}{\partial\,y} = \frac{1}{(\rho\,C_p)_{hnf}}\left(k_{hnf} + \frac{16\,\sigma^* T_\infty^3}{3\,k^*}\right)\frac{\partial^2 T}{\partial\,y^2}, \tag{6}$$

where σ^* and k^* represent the Stefan–Boltzmann constant and the mean absorption coefficient, respectively. Meanwhile, the pertaining boundary conditions for this flow problem are:

$$\left.\begin{array}{c} v = v_w(x,t) = 0,\;\; u = u_w(x,t) = 0, -k_{hnf}\frac{\partial T}{\partial y} = h_f\left(T_f - T\right) \quad \text{at} \quad y = 0 \\ u = u_e(x,t) \to \frac{a\,x}{1-c\,t},\;\; T \to T_\infty \;\; \text{at}\; y \to \infty \end{array}\right\}. \tag{7}$$

In the above equations and boundary conditions, (u, v) denote the velocity components along the (x, y)-axes, T is the temperature, g is the acceleration due to gravity, and h_f

is the convective heat transfer coefficient. In Equation (3), $\left[\pi\, j_0\, \widetilde{M}_0(x)\left(-\pi\frac{z}{p}\right)\right]/\left[8\,\rho_{hnf}\right]$ is the Grinberg term with $\widetilde{M}_0$ as the magnetization of the permanent magnets, p as the width of electrodes, and j_0 as the density applied in the electrodes.

Furthermore,

$$\left.\begin{array}{c}
\mu_{hnf} = \mu_{H_2O}\left(1-\phi_{Al_2O_3}-\phi_{Cu}\right)^{-2.5} \\
\rho_{hnf} = \phi_{Al_2O_3}\rho_{Al_2O_3} + \phi_{Cu}\rho_{Cu} + \left(1-\phi_{hnf}\right)\rho_{H_2O} \\
\frac{k_{hnf}}{k_{H_2O}} = \left\{\frac{\phi_{Al_2O_3}k_{Al_2O_3}+\phi_{Cu}k_{Cu}}{\phi_{Al_2O_3}+\phi_{Cu}} + 2k_{H_2O} + 2\left(\phi_{Al_2O_3}k_{Al_2O_3}+\phi_{Cu}k_{Cu}\right) - 2\left(\phi_{Al_2O_3}+\phi_{Cu}\right)k_{H_2O}\right\}\times \\
\left\{\frac{\phi_{Al_2O_3}k_{Al_2O_3}+\phi_{Cu}k_{Cu}}{\phi_{Al_2O_3}+\phi_{Cu}} + 2k_{H_2O} - \left(\phi_{Al_2O_3}k_{Al_2O_3}+\phi_{Cu}k_{Cu}\right) + \left(\phi_{Al_2O_3}+\phi_{Cu}\right)k_{H_2O}\right\}^{-1} \\
\left(\rho C_p\right)_{hnf} = \phi_{Al_2O_3}\left(\rho C_p\right)_{Al_2O_3} + \phi_{Cu}\left(\rho C_p\right)_{Cu} + \left(1-\phi_{hnf}\right)\left(\rho C_p\right)_{H_2O} \\
\left(\rho\beta\right)_{hnf} = \left(1-\phi_{hnf}\right)\left(\rho\beta\right)_{H_2O} + \phi_{Al_2O_3}\left(\rho\beta\right)_{Al_2O_3} + \phi_{Cu}\left(\rho\beta\right)_{Cu} \\
\text{where } \phi_{hnf} = \phi_{Al_2O_3} + \phi_{Cu}
\end{array}\right\} \tag{8}$$

These correlations for the hybrid nanofluid's density (ρ_{nhf}), dynamic viscosity (μ_{hnf}), thermal conductivity (k_{hnf}), heat capacity ($\left(\rho\, C_p\right)_{hnf}$), and thermal expansion coefficient (β_{hnf}) are plausible and true (see Takabi and Salehi [62]). Here, ϕ is the nanoparticle volume fraction and C_p stands for the heat capacity at constant pressure. This model is reduced to Cu/H_2O nanofluid if $\phi_{Al_2O_3} = 0\%$ and Al_2O_3/H_2O nanofluid if $\phi_{Cu} = 0\%$. In addition, a model for a viscous fluid is obtained when both $\phi_{Al_2O_3} = \phi_{Cu} = 0\%$. Table 1 lists the physical characteristics of water (H_2O), alumina (Al_2O_3), and copper (Cu).

Table 1. Thermal and physical characteristics for the base fluid and nanofluids (see Ahmed et al. [63]).

Physical Properties	ρ (kg/m^3)	C_p (J/kg K)	k (W/m K)
Cu	8933	385	400
Al_2O_3	3970	765	40
H_2O	997.1	4179	0.613

We now introduce the following appropriate transformations [58]:

$$\left.\begin{array}{c}
u = \frac{a\,x}{1-c\,t}f'(\eta),\;\; v = -\sqrt{\frac{a\,\nu_f}{1-c\,t}}f(\eta),\;\; \theta(\eta) = \frac{T-T_\infty}{T_f(x,t)-T_\infty}, \\
\eta = y\sqrt{\frac{a/\nu_f}{1-c\,t}}.
\end{array}\right\} \tag{9}$$

In order for Equations (2), (3) and (6) to reduce to ordinary differential equations (have similarity solutions), we assume that $\widetilde{M}_0(x,t) = [(x/l)\,M_0]/\left[(1-c\,t)^2\right]$, $\widetilde{b}(t) = (1-c\,t)^{-1/2}b, \widetilde{h}_f(t) = (1-ct)^{-1/2}h_f$, where M_0, b, and h_f are constant.

Then, we obtain the following differential equations after substituting the similarity variables (9) into Equations (2), (3) and (6):

$$\frac{\mu_{hnf}/\mu_{H_2O}}{\rho_{hnf}/\rho_{H_2O}}f''' + ff'' + 1 - f'^2 - A\left(f' + \frac{\eta}{2}f'' - 1\right) + \left(\frac{Z}{\frac{\rho_{hnf}}{\rho_{H_2O}}}\right)\mathrm{e}^{-b\,\eta} + \frac{\beta_{hnf}}{\beta_{H_2O}}\theta\lambda = 0, \tag{10}$$

$$\frac{1}{Pr}\,\frac{\left(\rho C_p\right)_{H_2O}}{\left(\rho C_p\right)_{hnf}}\left(\frac{k_{hnf}}{k_{H_2O}} + \frac{4}{3}R\right)\theta'' + f\,\theta' - \frac{1}{2}A\eta\theta' = 0, \tag{11}$$

subject to the boundary conditions

$$\left.\begin{array}{c}
f(0) = 0,\quad f'(0) = 0,\quad \theta'(0) = -\frac{k_{H_2O}}{k_{hnf}}Bi[1-\theta(0)], \\
f'(\eta)\to 1,\quad \theta(\eta)\to 0 \qquad \text{as} \qquad \eta\to\infty.
\end{array}\right\} \tag{12}$$

Here, Z stands for the modified Hartmann number, Pr for the Prandtl number, b for the parameter associated with the magnets and electrode width, A for the unsteadiness parameter, R for the radiation parameter, λ for the mixed convection parameter, and Bi for the Biot number, which are defined by:

$$Pr = \frac{(\mu C_p)_{H_2O}}{k_{H_2O}}, \quad Z = \frac{\pi\, j_0\, M_0}{8\, a^2 l \rho_{H_2O}}, \quad b = \frac{\pi}{p}\sqrt{\frac{\nu_{H_2O}}{a}}, \quad A = \frac{c}{a},$$
$$R = \frac{4\,\sigma^*\,T_\infty^3}{k_{H_2O}\,k^*}, \quad \lambda = \frac{Gr_x}{Re_x^2}, \quad Bi = \frac{h_f}{k_{H_2O}}\sqrt{\frac{\nu_{H_2O}}{a}},$$

with $Gr_x = g\ \beta_{H_2O}\left[T_f(x,t) - T_\infty\right]\ x^3/{\nu_{H_2O}}^2$ and $Re_x = u_e(x,t)\ x/\nu_{H_2O}$ as the local Grashof number and local Reynolds number, respectively.

In the present work, we assume the Riga plate has an $A \leq 0$ and is deceleratingly shrinking. The EMHD parameter $Z > 0$ symbolizes the movement of the Lorentz force towards the positive $y-$ axis, while $Z < 0$ acts contradictorily. When $Z = 0$, the Riga plate acts as an axial flow.

Meanwhile,

$$C_f = \frac{\mu_{hnf}}{\rho_{H_2O}\,u_e^2(x,t)}\left(\frac{\partial\, u}{\partial\, y}\right)_{y=0}, \quad Nu_x = -\frac{x}{k_{H_2O}\left(T_f - T_\infty\right)}\left[\left(k_{hnf}\,\frac{\partial\, T}{\partial\, y}\right)_{y=0} + (q_r)_{y=0}\right], \tag{13}$$

are the local skin friction coefficient C_f and the local Nusselt number Nu_x. Using (9) and (13), we get:

$$Re_x^{1/2}\,C_f = \frac{\mu_{hnf}}{\mu_{H_2O}} f''(0), \quad Re_x^{-1/2} Nu_x = \left(\frac{k_{hnf}}{k_{H_2O}} + \frac{4}{3}\,R\right)\left[-\theta'(0)\right]. \tag{14}$$

For $\phi = 0$ (classical viscous fluid), $A = 0$ (steady state flow), $R = 0$, and $Z = 0$ (flat plate), Equations (10) and (12) reduce to:

$$f''' + ff'' + 1 - {f'}^2 + \theta\lambda = 0, \tag{15}$$

$$\theta'' + Prf\theta' = 0, \tag{16}$$

$$\left.\begin{array}{c} f(0) = 0, \quad f'(0) = 0, \quad \theta'(0) = -Bi[1 - \theta(0)] \\ f'(\eta) \to 1, \quad \theta(\eta) \to 0 \quad \text{as} \quad \eta \to \infty \end{array}\right\}. \tag{17}$$

The boundary value problem (15 to 17) is identical to the boundary value problems (8–10) from Jafar et al. [64] and the boundary value problem (7–10) from Mohamed et al. [65], when $M = \varepsilon = 0$. Therefore, we can compare our results with the papers mentioned above (see Table 2).

Table 2. Comparison of results with those by Jafar et al. [64] and Mohamed et al. [65].

Pr	*Bi*	$Re_x^{1/2}\,C_f$		$Re_x^{-1/2}Nu_x$		Percentage Difference (%)
		Present Result	Mohamed et al. [65]	Present Result	Jafar et al. [64]	
0.72	0.05	1.2325876	1.2325877	0.045466	0.045466	8.11301×10^{-6}
	0.1	1.2325876	1.2325877	0.083373	0.083373	8.11301×10^{-6}
	0.2	1.2325876	1.2325877	0.142974	0.142974	8.11301×10^{-6}

3. Stability Analysis

We tested whether the dual solutions of the boundary value problem (10 to 12) are stable or unstable by performing a stability analysis. In this respect, we followed Merkin [66] or Weidman et al. [67], who have shown that the lower branch solutions are unstable (not physically realizable in practice), while the upper branch solutions are stable (physically realizable in practice). As in Weidman et al. [67], we introduce the new dimensionless time

variable τ. The use of τ is associated with an initial value problem and is consistent with the question of which obtained solution is stable (physically realizable). We now have:

$$\left.\begin{array}{c} u = \frac{a\,x}{1-c\,t}\frac{\partial f}{\partial \eta}(\eta,\tau),\;\; v = -\sqrt{\frac{a\,\nu_f}{1-c\,t}}f(\eta,\tau) \\ \theta(\eta,\tau) = \frac{T-T_\infty}{T_f(x,t)-T_\infty},\;\; \eta = y\sqrt{\frac{a/\nu_f}{1-c\,t}} \end{array}\right\}, \tag{18}$$

so that Equations (3) and (6) become:

$$\begin{array}{c} \frac{\mu_{hnf}/\mu_{H_2O}}{\rho_{hnf}/\rho_{H_2O}}\frac{\partial^3 f}{\partial \eta^3} + f\frac{\partial^2 f}{\partial \eta^2} + 1 - \left(\frac{\partial f}{\partial \eta}\right)^2 - A\left(\frac{\partial f}{\partial \eta} + \frac{\eta}{2}\frac{\partial^2 f}{\partial \eta^2} - 1\right) + \left(\frac{Z}{\rho_{hnf}/\rho_{H_2O}}\right)e^{-b\,\eta} \\ + \frac{\beta_{hnf}}{\beta_{H_2O}}\theta\lambda - (1+A\tau)\frac{\partial^2 f}{\partial \eta \partial \tau} = 0, \end{array} \tag{19}$$

$$\frac{1}{Pr}\frac{(\rho C_p)_{H_2O}}{(\rho C_p)_{hnf}}\left(\frac{k_{hnf}}{k_{H_2O}} + \frac{4}{3}R\right)\frac{\partial^2 \theta}{\partial \eta^2} + f\frac{\partial \theta}{\partial \eta} - \frac{1}{2}A\eta\frac{\partial \theta}{\partial \eta} - (1+A\tau)\frac{\partial \theta}{\partial \tau} = 0, \tag{20}$$

with boundary conditions of:

$$\left.\begin{array}{c} f(0,\tau) = 0,\quad \frac{\partial f}{\partial \eta}(0,\tau) = 0,\quad \frac{\partial \theta}{\partial \eta}(0,\tau) = -\frac{k_{H_2O}}{k_{hnf}}Bi[1-\theta(0,\tau)] \\ \frac{\partial f}{\partial \eta}(\eta,\tau) \to 1,\quad \theta(\eta,\tau) \to 0 \quad \text{as} \quad \eta \to \infty \end{array}\right\}. \tag{21}$$

Initial decay or growth of disturbance in the steady solutions $f_0(\eta)$ and $\theta_0(\eta)$ determines the stability of the solutions [67]. Therefore, the following perturbation functions containing disturbance that changes exponentially with time (see Weidman et al. [67]):

$$\left.\begin{array}{c} f(\eta,\tau) = f_0(\eta) + e^{-\gamma\tau}\,F(\eta,\tau) \\ \theta(\eta,\tau) = \theta_0(\eta) + e^{-\gamma\tau}\,M(\eta,\tau) \end{array}\right\}, \tag{22}$$

are substituted into Equations (19) to (21). In the preceding functions, γ represents the unknown eigenvalue, and $f_0(\eta)$ and $\theta_0(\eta)$ are large in comparison to $F(\eta,\tau)$ and $M(\eta,\tau)$, respectively. By setting the value $\tau = 0$,

$$\frac{\mu_{hnf}/\mu_{H_2O}}{\rho_{hnf}/\rho_{H_2O}}F_0''' + f_0F_0'' + F_0f_0'' - 2f_0'F_0' - AF_0' - \frac{A}{2}\eta F_0'' + \frac{\beta_{hnf}}{\beta_{H_2O}}\lambda M_0 + \gamma F_0' = 0, \tag{23}$$

$$\frac{1}{Pr}\frac{(\rho C_p)_{H_2O}}{(\rho C_p)_{hnf}}\left(\frac{k_{hnf}}{k_{H_2O}} + \frac{4}{3}R\right)M_0'' + f_0M_0' + F_0\theta_0' - \frac{A}{2}\eta M_0' + \gamma M_0 = 0, \tag{24}$$

$$\left.\begin{array}{c} F_0(0) = 0,\quad F_0'(0) = 0,\quad M_0'(0) = \frac{k_{H_2O}}{k_{hnf}}BiM_0(0) \\ F_0'(\eta) \to 0,\quad M_0(\eta) \to 0 \quad \text{as} \quad \eta \to \infty \end{array}\right\}. \tag{25}$$

To allow the evaluation of the smallest eigenvalue γ_1, one of the homogenous far-field boundary conditions (25) (i.e., $F_0'(\eta) \to 0$) is relaxed to yield $F_0''(0) = 1$ [68]. The stable and unstable solutions are represented by the positive and negative values of γ_1.

4. Results and Discussion

The MATLAB solver bvp4c, which has a finite difference code, generated all the numerical results in this work. For computation purposes, appropriate substitutions are made to rewrite Equations (10) to (12) as first-order ordinary differential equations. A brief example of this step of the computation is described by Yahaya et al. [69]. Before further computations are made using the MATLAB solver, the mathematical framework and approach employed in this study are validated by comparing them to the previously published papers by Jafar et al. [64] and Mohamed et al. [65]. As can be seen from Table 2, our results are in excellent agreement with the results mentioned above. Therefore, we are deeply confident that the present results are accurate and correct.

The impacts of several pertinent parameters on the flow and heat transfer behaviors of the hybrid nanofluid were scrutinized. Throughout this study, $Pr = 6.2$ for water, and $\phi_{Al_2O_3}$ and ϕ_{Cu} were maintained at 0.02. The far-field region of $\eta_{\max}$ was adjusted to 10 for the velocity and temperature profiles, which asymptotically achieved the far-field boundary condition (12). The bvp4c function requires an initial guess of the solution for the boundary values problem (10 to 12). The guess must satisfy the boundary conditions (12) and keep the behavior of the solution. Determining an initial guess for the first (upper branch) solution is not difficult because the bvp4c method will converge to the first solution even for poor guesses. However, it is rather difficult to determine a sufficiently good guess for the second (lower branch) solution of the boundary value problem (10 to 12). In this case, we used the technique called continuation [70]. As explained in the previous section, the computation of linearized eigenvalue problems (23) to (25) subjected to the new boundary condition will produce an infinite set of eigenvalues (i.e., $\gamma_1 < \gamma_2 < \gamma_3 < \cdots$). The value of γ_1 will determine the stability of the solutions, and the results are tabulated in Table 3. As observed from this table, the first solution has positive γ_1 values, that denote a meaningful and stable solution (physically realizable in practice). The second solution, with negative values of γ_1, is identified as unstable but still holds mathematical importance. Therefore, the discussion here is based on the physically realizable first solution. Nevertheless, the second solution was still be recorded.

Table 3. Smallest eigenvalue, γ_1 for $Pr = 6.2$, $A = -0.5$, $\phi_{Al_2O_3} = \phi_{Cu} = 0.02$, $b = Z = Bi = 0.5$, and $R = 1.3$.

λ	γ_1	
	First Solution	**Second Solution**
−1.0	0.97587	−1.51783
−0.5	1.86571	−1.78683
0.9	0.89239	−0.06152
1.0	0.88626	−0.06402

We notice that all Figures 2–10 show that unique solutions exist for the boundary value problem (10 to 12) when $\lambda > 0$ (assisting flow), dual solutions (upper and lower branch solutions) exist for $\lambda_c < \lambda < 0$ (opposing flow) and no solutions exist for $\lambda < \lambda_c < 0$ where $\lambda_c < 0$ is the critical value of $\lambda < 0$ for which the boundary value problem (10 to 12) have no solutions. It should be stated that for $\lambda < \lambda_c < 0$ the full Navier–Stokes and energy Equations (2) to (4) have to be solved.

The plots of physical quantities of interest with the unsteadiness parameter A and mixed convection parameter λ are given in Figure 2. Both solutions of $Re_x^{1/2}\, C_f$ showed a reducing trend with the increasing magnitude of A (see Figure 2a). Meanwhile, the increment of λ augmented the value of $Re_x^{1/2}\, C_f$, which denotes the rise of the skin friction coefficient. A slight improvement of $Re_x^{-1/2} Nu_x$ by λ was also observed in Figure 2b. This behavior is due to the enhancement of temperature gradient $-\theta\prime(0)$. In addition, the increase in $|A|$ raised the values of $Re_x^{-1/2} Nu_x$, which are proportional to the heat transfer rate.

Figure 3 depicts the behavior of the skin friction coefficient and Nusselt number with varying values of the modified Hartmann number Z. Both the opposing ($\lambda < 0$) and aiding ($\lambda > 0$) flows exhibited an amplified skin friction coefficient as Z increased (see Figure 3a). Similar behavior was also seen for $Re_x^{-1/2} Nu_x$ in Figure 3b. The rise in heat transfer rate by Z indicates better cooling is achieved. Meanwhile, Figure 4 shows the variation of $Re_x^{1/2}\, C_f$ and $Re_x^{-1/2} Nu_x$ with b and Z. In both Figure 4a,b, two different behaviors were obtained for the opposing ($Z < 0$) and aiding ($Z > 0$) the Lorentz force when the magnets and electrode width parameter b increased. For negative values of Z, the enhancement of b augmented the values of $Re_x^{1/2}\, C_f$ and $Re_x^{-1/2} Nu_x$. However, the opposite trend was obtained for positive values of Z.

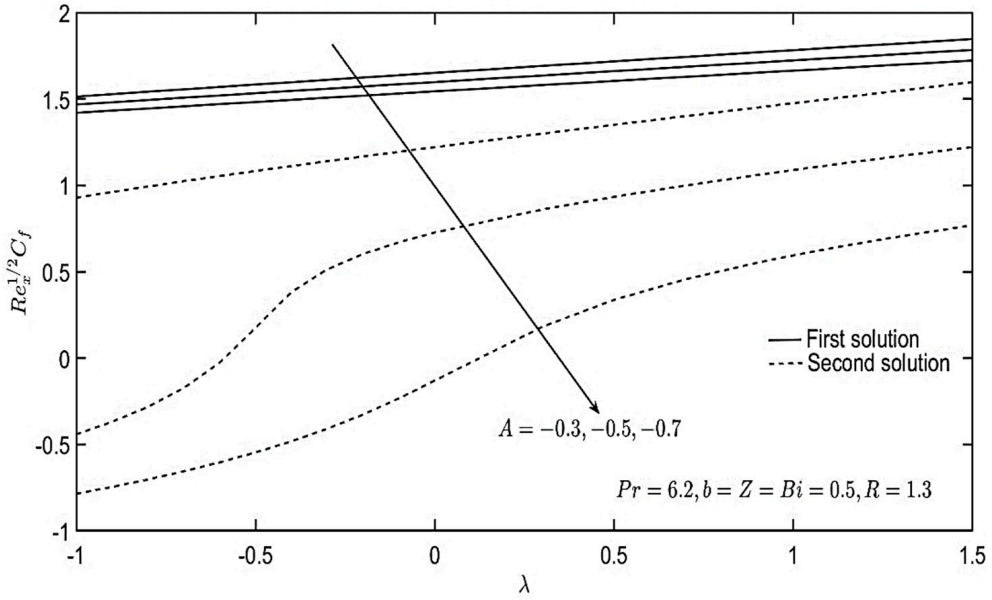

(**a**)

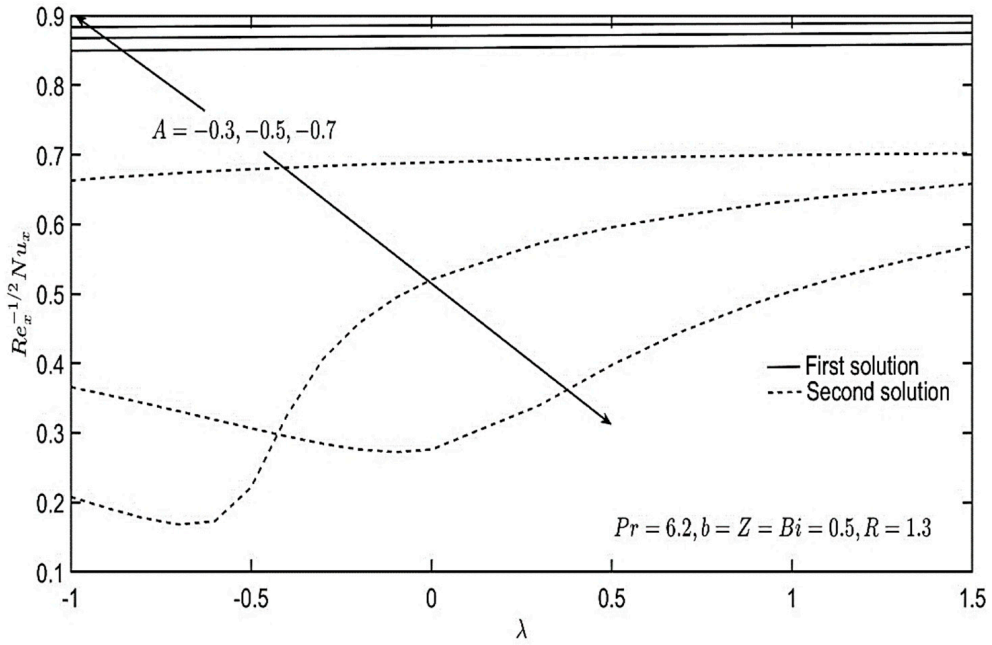

(**b**)

Figure 2. Plots of (**a**) $Re_x^{1/2}\, C_f$ and (**b**) $Re_x^{-1/2} Nu_x$ with various values of A and λ.

Further, Figure 5 illustrates the impacts of A on the velocity and temperature profiles. The velocity profile around the plate diminished with the increase in $|A|$ (see Figure 5a). The boundary layer thickened and reduced the velocity gradient (i.e., $f''(0)$), which further decreased the value of $Re_x^{1/2}\, C_f$, as shown in Figure 2a. Interestingly, the velocity profile of the hybrid nanofluid, located far from the plate, showed an increasing trend with $|A|$. In contrast, a rise in $|A|$ reduced the temperature profile and reduced the thermal boundary layer (see Figure 5b). The temperature gradient at the Riga plate's surface then increased, boosting the $Re_x^{-1/2} Nu_x$.

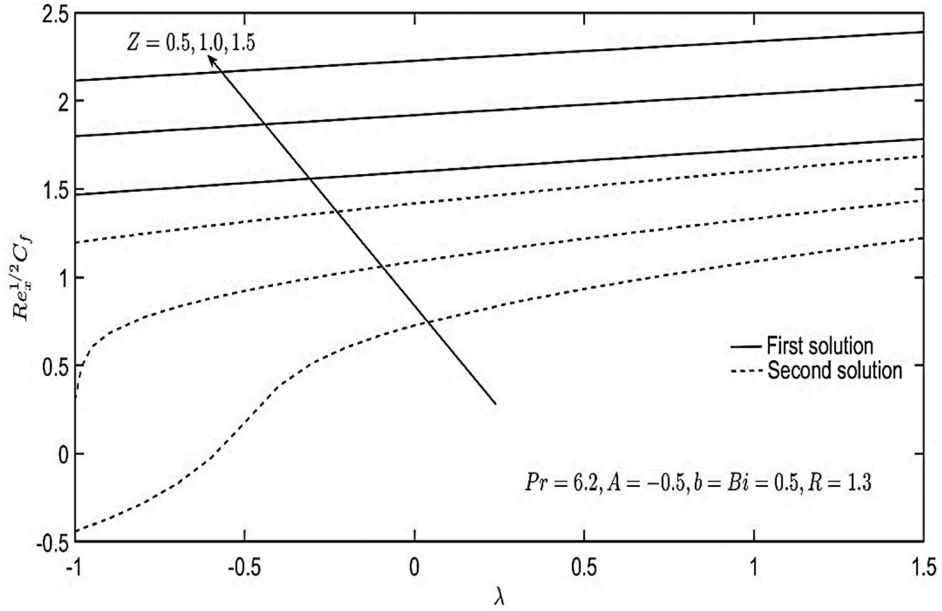

(**a**)

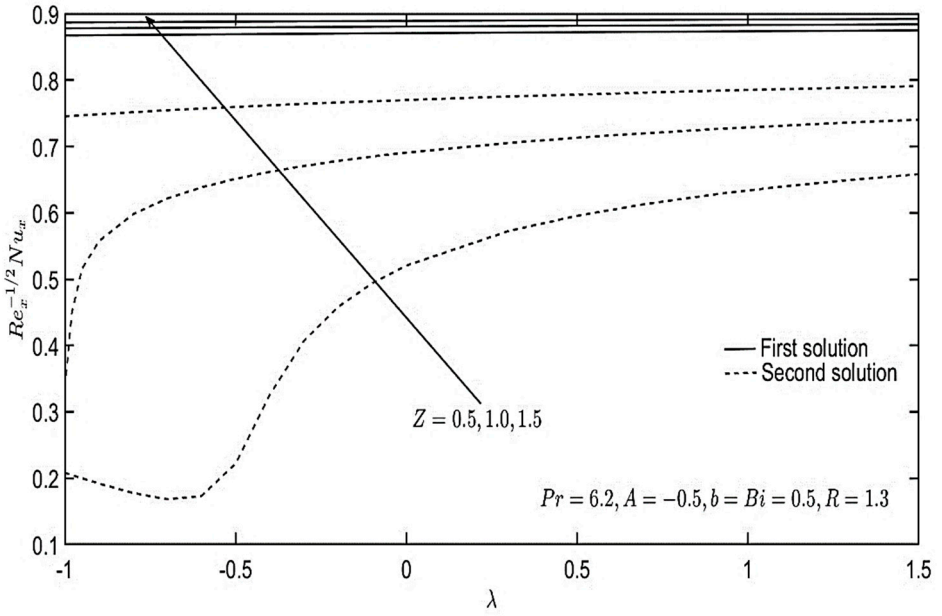

(**b**)

Figure 3. Plots of (**a**) $Re_x^{1/2}\, C_f$ and (**b**) $Re_x^{-1/2} Nu_x$ with various values of Z and λ.

Next, Figure 6 illustrates the velocity and temperature profiles with the effects of the mixed convection parameter λ. The opposing flow or heating problem is represented by $\lambda < 0$ such that $T_f < T_\infty$, while $\lambda > 0$ denotes an assisting flow or cooling problem for $T_f > T_\infty$. Based on Figure 6a, the increase in λ was observed to improve the hybrid nanofluid's velocity profile and to thin the momentum boundary layer. The increase of the mixed convection parameter λ promoted the enhancement of the free convection parameter Gr_x. Hence, the buoyancy force rose and boosted the hybrid nanofluid flow. The velocity gradient increased and raised $Re_x^{1/2}\, C_f$, as seen in Figure 2a. However, a decreasing trend was seen for the temperature profile in Figure 6b when λ increased. The augmentation of λ decreased the thermal diffusivity of the hybrid nanofluid (see Ibrahim and Anbessa [71]). As a result, the thermal boundary layer became thinner (see Figure 6b).

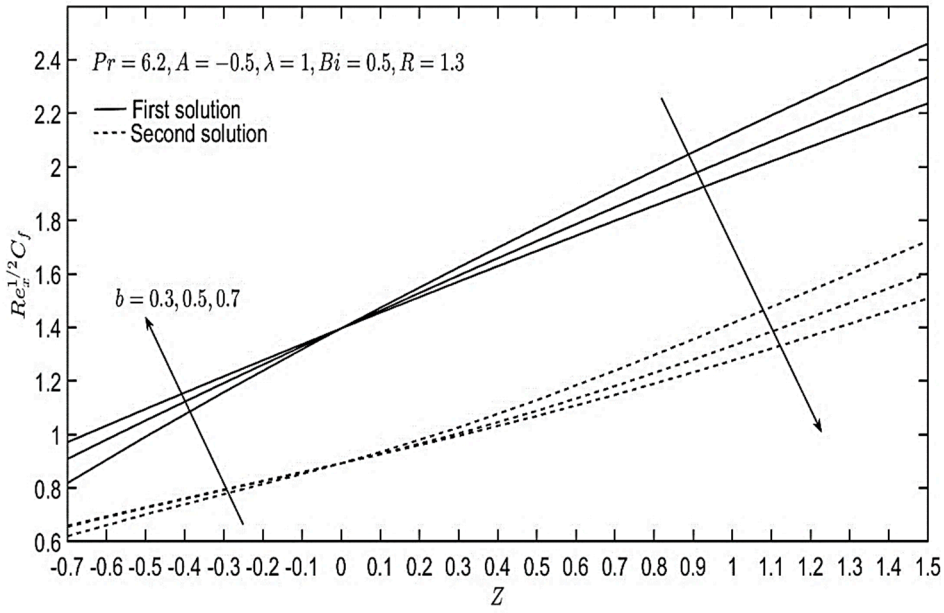

(**a**)

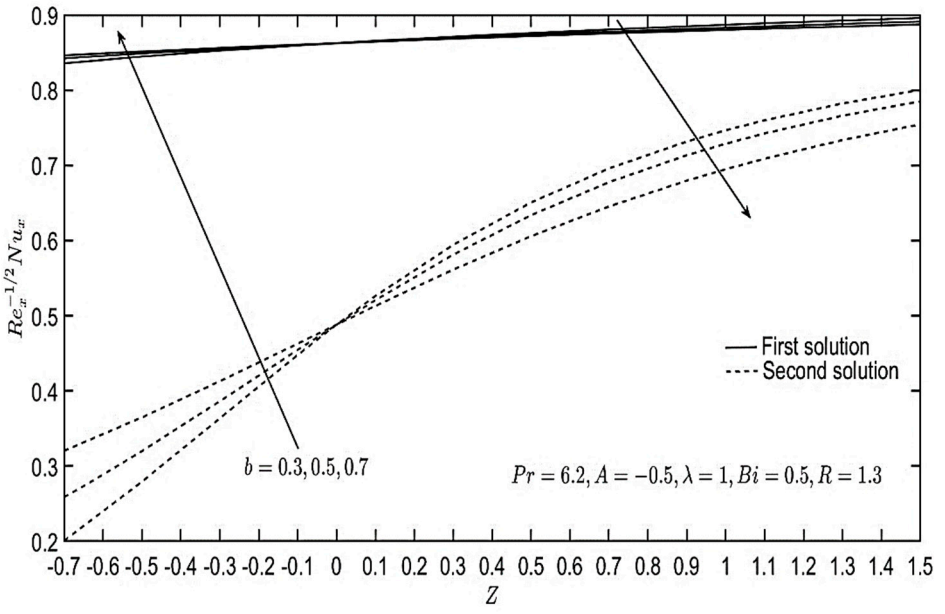

(**b**)

Figure 4. Plots of (**a**) $Re_x^{1/2}\, C_f$ and (**b**) $Re_x^{-1/2} Nu_x$ with various values of b and Z.

The velocity profile was also enhanced by the increase in the modified Hartmann number Z. Physically, the increase in Z was associated with the increment of the electrical field that generates the Lorentz force [60]. This force then retarded the boundary layer and raised the velocity profile, as obtained in Figure 7a. Further increase in Z then promoted the overshot of the velocity profiles (see Figure 7a), which indicates that the velocity of the hybrid nanofluid near the Riga plate exceeded the free stream velocity under strong Lorentz forces. Meanwhile, the thermal boundary layer constricted as Z increased. Then, a subsequent decrease in the temperature profile was seen (see Figure 7b). Ganesh et al. [72] and Nayak et al. [73] reported the same behavior.

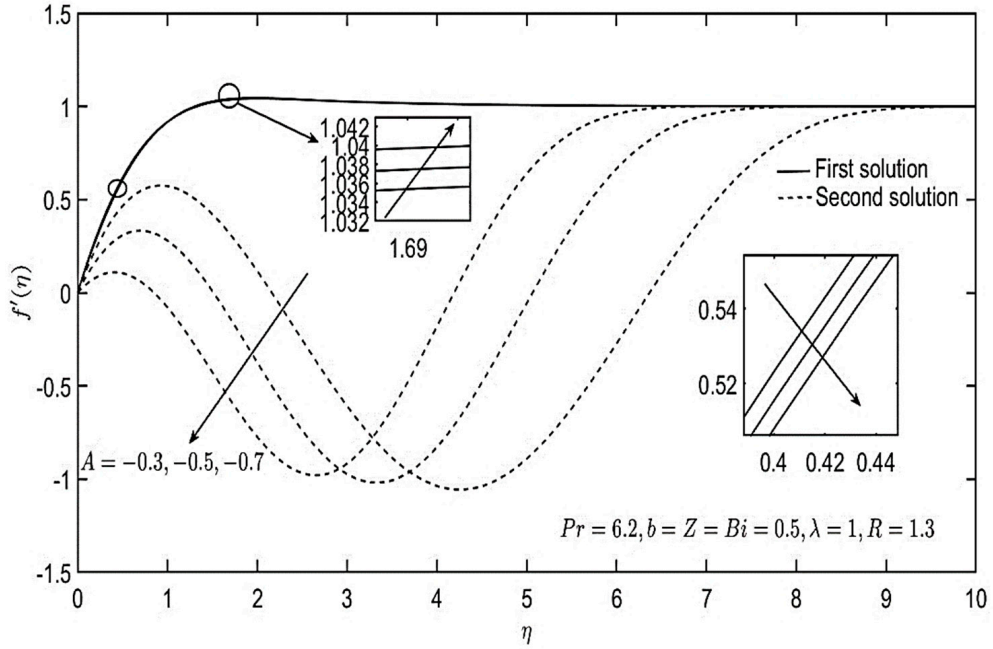

(**a**)

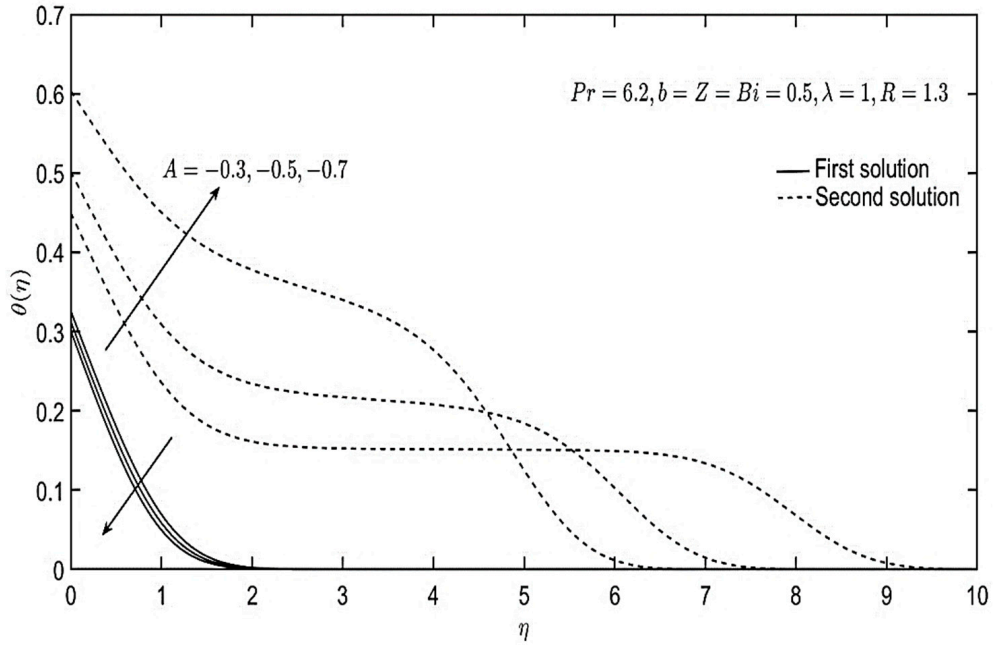

(**b**)

Figure 5. (**a**) Velocity and (**b**) temperature distributions for various values of A.

Other than that, the effects of the magnets and electrode width were analyzed through the dimensionless parameter b. The results presented in Figure 8 suggest that the increment of b reduced and increased the velocity and temperature profiles, respectively. In addition, it can be noticed that the increase in b promoted the growth of momentum and thermal boundary layers (see Figure 8a,b). However, the increase in b reduced the gradients of velocity and temperature (i.e., $f''(0)$) and $-\theta'(0)$), which lowered the magnitudes of $Re_x^{1/2}\, C_f$ and $Re_x^{-1/2} Nu_x$ (see Figure 4a,b).

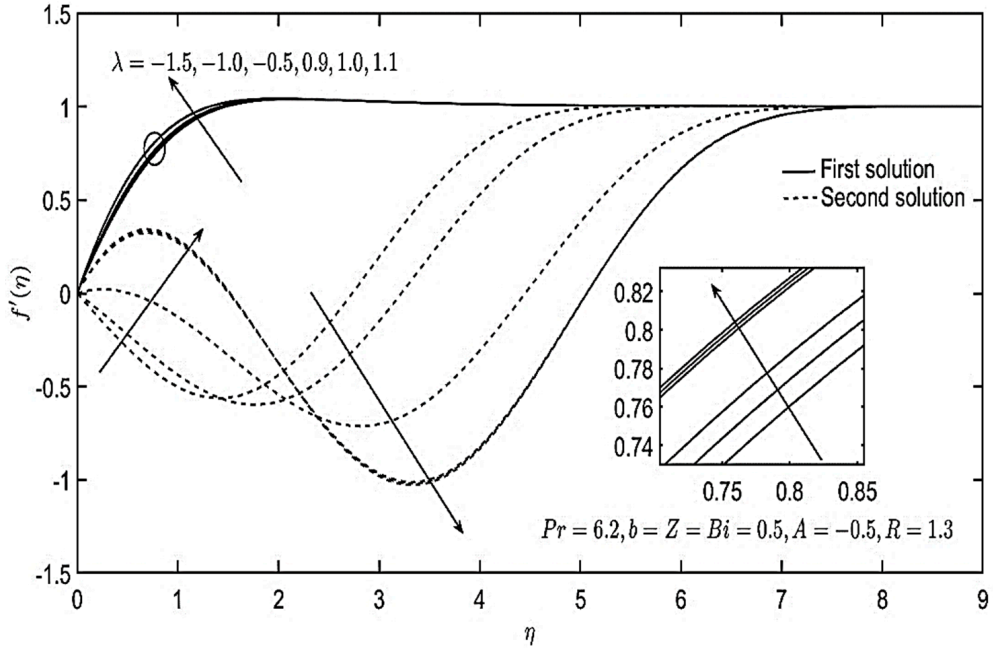

(**a**)

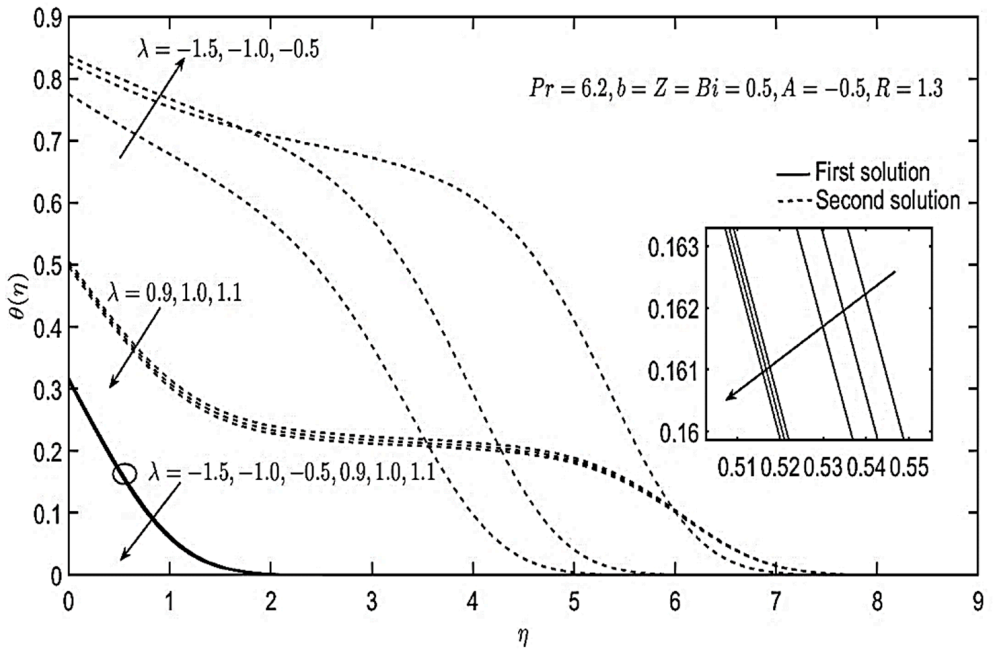

(**b**)

Figure 6. (**a**) Velocity and (**b**) temperature distributions for various values of λ.

Finally, a parameter related to the convective boundary condition, Bi, directly correlated with the convective heat transfer coefficient h_f. Therefore, the augmentation of the Biot number boosted the convective heat transfer between the plate and the hybrid nanofluid, raised the temperature profile of the hybrid nanofluid, and thickened the boundary layer, as observed in Figure 9. Likewise, the existence of radiation in the flow resulted in the same impacts towards the boundary layer and temperature distribution (see Figure 10).

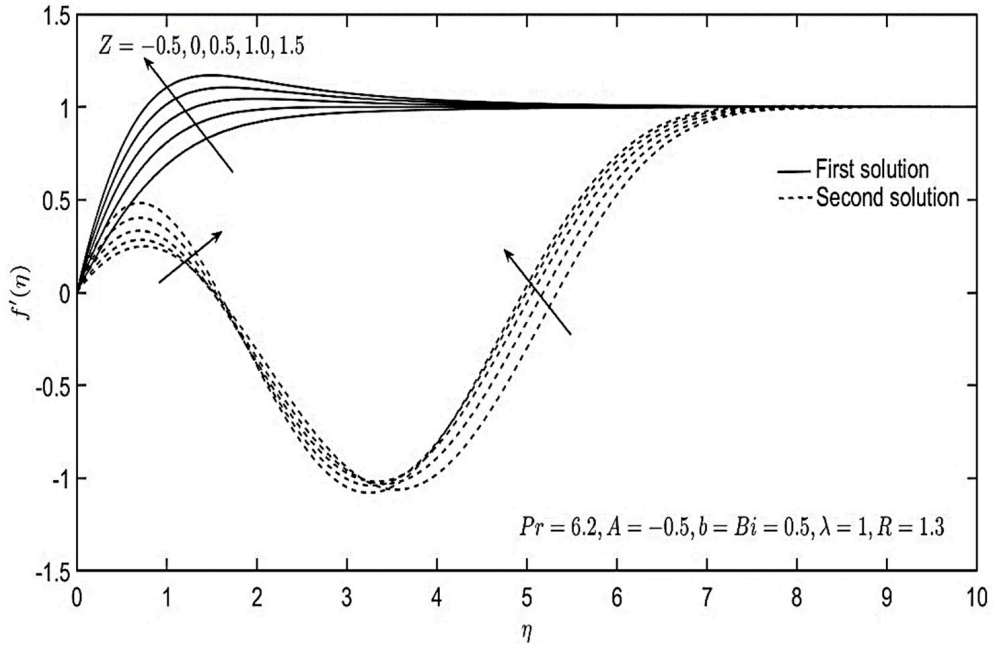

(**a**)

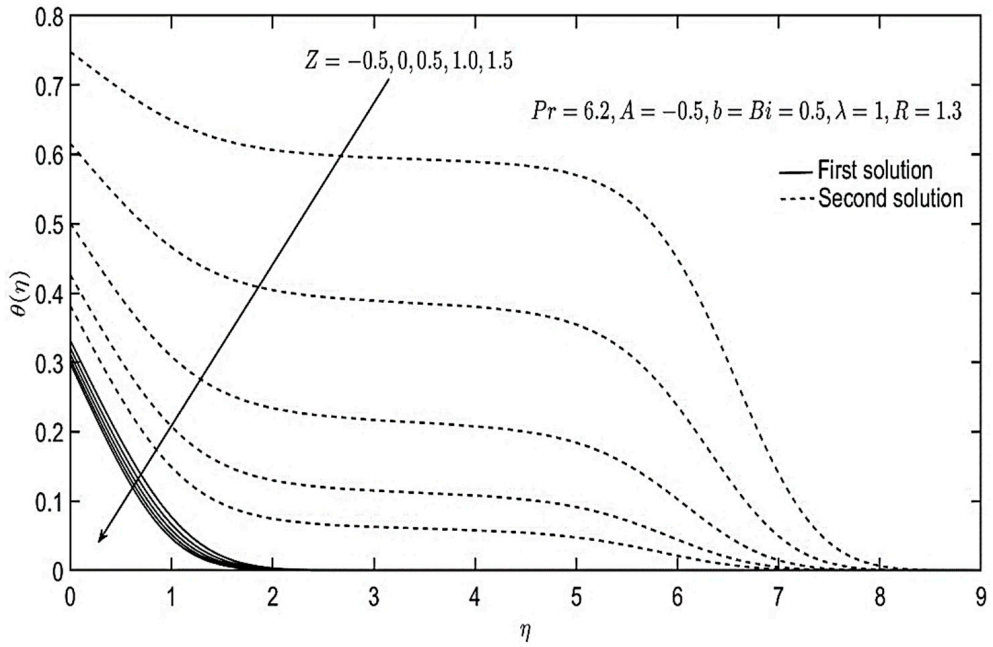

(**b**)

Figure 7. (**a**) Velocity and (**b**) temperature distributions for various values of Z.

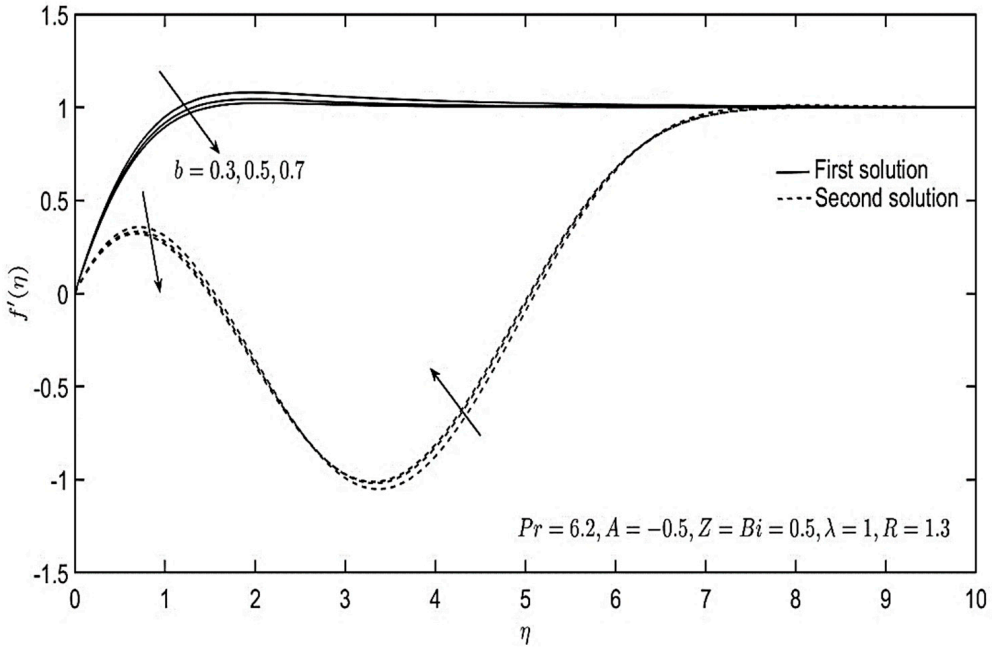

(**a**)

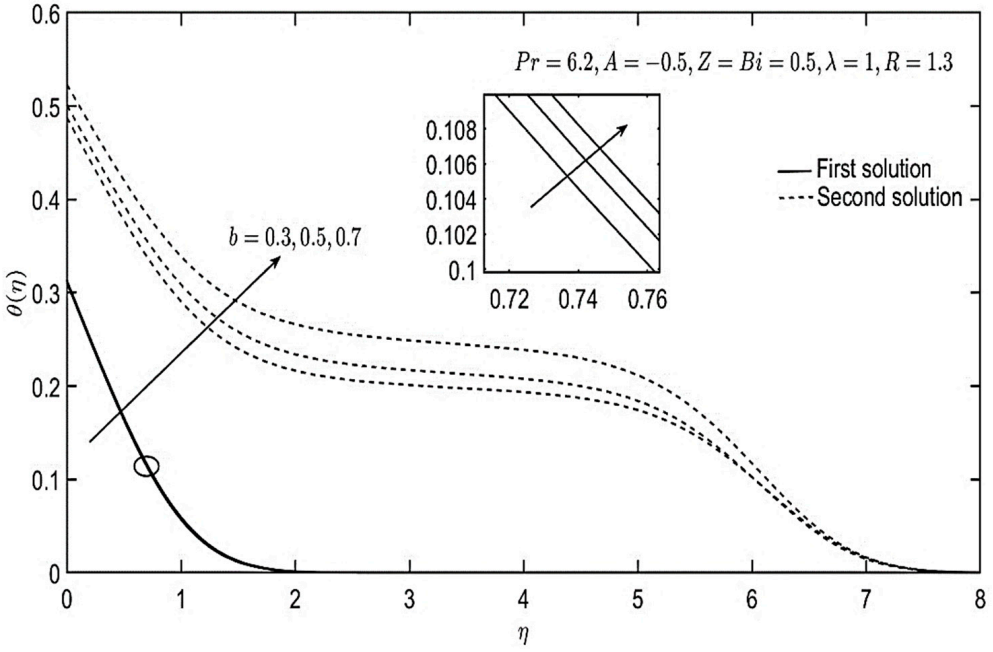

(**b**)

Figure 8. (**a**) Velocity and (**b**) temperature distributions for various values of b.

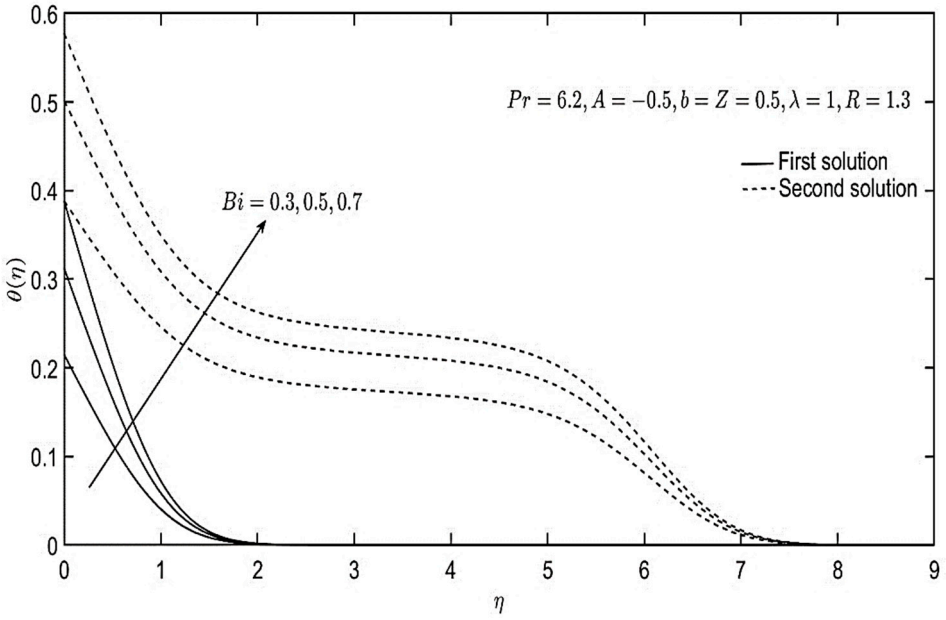

Figure 9. Temperature distributions for various values of Bi.

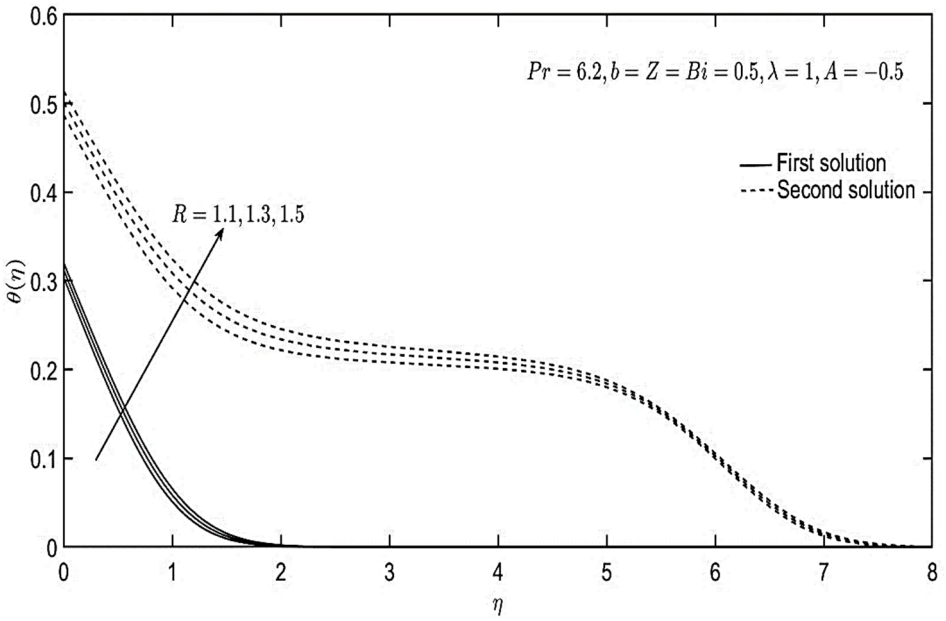

Figure 10. Temperature distributions for various values of R.

5. Conclusions

The mathematical formulation for the unsteady two-dimensional hybrid nanofluid's flow, induced by mixed convection, across a Riga plate with radiation and convective boundary condition was presented. The problem was solved numerically using the bvp4c solver in MATLAB. Dual solutions in the computation prompted a stability analysis that successfully identified the first solution as stable and physically meaningful. In addition, the effects of other controlling parameters were scrutinized.

The increase in the unsteadiness parameter reduced the skin friction coefficient and improved the Nusselt number. Meanwhile, enhancing the mixed convection parameter and modified Hartmann number augmented the skin friction coefficient and Nusselt number. In addition, increasing the magnets and electrode width parameter in opposing Lorentz force enhanced these physical quantities of interest. Still, the opposite trend was obtained with the aiding Lorentz force. Through the numerical computations, is was

indicated that the heat transfer performance can be improved using the Riga plate with the augmentation of the modified Hartmann number, mixed convection parameter, and unsteadiness parameter. However, the increment of the modified Hartmann number and mixed convection parameter raised the wall shear stress.

The current study emphasized providing the numerical solution for the mathematical formulation of the stated flow problem. Then, a stability analysis was performed to aid the process of choosing a stable, physically realizable solution in actual practice. This current study can be extended into an experimental study or supplied with modifications to suit real-life applications.

Author Contributions: Conceptualization, I.P.; methodology, I.P. and R.I.Y.; validation, I.P. and N.M.A.; formal analysis, R.I.Y.; writing—original draft preparation, R.I.Y. and I.P.; writing—review and editing, N.M.A. and I.P.; supervision, N.M.A., F.M.A., and S.S.P.M.I.; funding acquisition, N.M.A. All authors have read and agreed to the published version of the manuscript.

Funding: The authors gratefully acknowledge the financial support from the Universiti Putra Malaysia (grant number GP-GPB 9711400). The work of Ioan Pop has been supported from the UEFISCDI, Romania (Grant PN-III-P4-PCE-2021-0993).

Institutional Review Board Statement: Not applicable.

Informed Consent Statement: Not applicable.

Conflicts of Interest: The authors declare no conflict of interest.

Nomenclature

a, c	constant
A	unsteadiness parameter
b	parameter related to magnets and electrode width
Bi	Biot number
C_f	skin friction coefficient
C_p	heat capacity (J/kgK)
f	dimensionless velocity
g	acceleration due to gravity (m/s^2)
Gr_x	local Grashof number
h_f	convective heat transfer coefficient
j_0	density applied in the electrodes
k	thermal conductivity (W/m·K)
k^*	mean absorption coefficient
l	characteristic length
$\widetilde{M}_0$	magnetization of permanent magnets
Nu_x	local Nusselt number
p	width of electrodes
Pr	Prandtl number
q_r	radiation heat flux
R	radiation parameter
Re_x	local Reynolds number
t	time (s)
T	fluid temperature (K)
T_f	convective temperature
T_0	characteristic temperature
T_∞	far-field temperature
x, y	Cartesian coordinates (m)
u, v	velocity components(m/s)
u_e	far-field velocity (m/s)
u_e	far-field velocity (m/s)
Z	modified Hartmann number

Greek symbols

ν	kinematic viscosity (m^2/s)
β	thermal expansion coefficient
ψ	stream function
λ	mixed convection parameter
σ^*	Stefan–Boltzmann constant
γ	unknown eigenvalue
τ	dimensionless time variable
η	similarity variable
θ	dimensionless temperature
ρ	fluid density (kg/m^3)
ϕ	nanoparticle volume fraction
μ	dynamic viscosity (kg/m^2s)

References

1. Eshgarf, H.; Afrand, M. An experimental study on rheological behavior of non-Newtonian hybrid nano-coolant for application in cooling and heating systems. *Exp. Therm. Fluid Sci.* **2016**, *76*, 221–227. [CrossRef]
2. Wahid, N.S.; Arifin, N.M.; Khashi'ie, N.S.; Pop, I.; Bachok, N.; Hafidzuddin, M.E.H. Flow and heat transfer of hybrid nanofluid induced by an exponentially stretching/shrinking curved surface. *Case Stud. Therm. Eng.* **2021**, *25*, 100982. [CrossRef]
3. Shao, X.F.; Mo, S.P.; Chen, Y.; Yin, T.; Yang, Z.; Jia, L.S.; Cheng, Z.D. Solidification behavior of hybrid TiO2 nanofluids containing nanotubes and nanoplatelets for cold thermal energy storage. *Appl. Therm. Eng.* **2017**, *117*, 427–436. [CrossRef]
4. Dubal, D.P.; Rueda-Garcia, D.; Marchante, C.; Benages, R.; Gomez-Romero, P. Hybrid graphene-polyoxometalates nanofluids as liquid electrodes for dual energy storage in novel flow cells. *Chem. Rec.* **2018**, *18*, 1076–1084. [CrossRef]
5. Vaka, M.; Walvekar, R.; Khalid, M.; Jagadish, P.; Mubarak, N.M.; Panchal, H. Synthesis of hybrid graphene/TiO2 nanoparticles based high-temperature quinary salt mixture for energy storage application. *J. Energy Storage* **2020**, *31*, 101540. [CrossRef]
6. Selimefendigil, F.; Öztop, H.F. Impacts of magnetic field and hybrid nanoparticles in the heat transfer fluid on the thermal performance of phase change material installed energy storage system and predictive modeling with artificial neural networks. *J. Energy Storage* **2020**, *32*, 101793. [CrossRef]
7. Gao, Y.; An, J.; Xi, Y.; Yang, Z.; Liu, J.; Mujumdar, A.S.; Wang, L.; Sasmito, A.P. Thermal conductivity and stability of novel aqueous graphene oxide–Al_2O_3 hybrid nanofluids for cold energy storage. *Appl. Sci.* **2020**, *10*, 5768. [CrossRef]
8. Maleki, Y.; Mehrpooya, M.; Pourfayaz, F. Cold thermal energy storage by encapsulated phase change materials system using hybrid nanofluids as the heat transfer fluid. *Int. J. Energy Res.* **2021**, *45*, 15265–15283. [CrossRef]
9. Alrowaili, Z.A.; Ezzeldien, M.; Shaaalan, N.M.; Hussein, E.; Sharafeldin, M.A. Investigation of the effect of hybrid CuO-Cu/water nanofluid on the solar thermal energy storage system. *J. Energy Storage* **2022**, *50*, 104675. [CrossRef]
10. Turcu, R.; Darabont, A.L.; Nan, A.; Aldea, N.; Macovei, D.; Bica, D.; Vekas, L.; Pana, O.; Soran, M.L.; Koos, A.A.; et al. New polypyrrole-multiwall carbon nanotubes hybrid materials. *J. Optoelectron. Adv. Mater.* **2006**, *8*, 643–647.
11. Jana, S.; Salehi-Khojin, A.; Zhong, W.H. Enhancement of fluid thermal conductivity by the addition of single and hybrid nano-additives. *Thermochim. Acta* **2007**, *462*, 45–55. [CrossRef]
12. Suresh, S.; Venkitaraj, K.P.; Selvakumar, P.; Chandrasekar, M. Synthesis of Al_2O_3–Cu/water hybrid nanofluids using two step method and its thermo physical properties. *Colloids Surf. A Physicochem. Eng. Asp.* **2011**, *388*, 41–48. [CrossRef]
13. Huminic, G.; Huminic, A. Hybrid nanofluids for heat transfer applications—A state-of-the-art review. *Int. J. Heat Mass Transf.* **2018**, *125*, 82–103. [CrossRef]
14. Sarkar, J.; Ghosh, P.; Adil, A. A review on hybrid nanofluids: Recent research, development and applications. *Renew. Sustain. Energy Rev.* **2015**, *43*, 164–177. [CrossRef]
15. Babu, J.A.R.; Kumar, K.K.; Rao, S.S. State-of-art review on hybrid nanofluids. *Renew. Sustain. Energy Rev.* **2017**, *77*, 551–565. [CrossRef]
16. Eshgarf, H.; Kalbasi, R.; Maleki, A.; Shadloo, M.S. A review on the properties, preparation, models and stability of hybrid nanofluids to optimize energy consumption. *J. Therm. Anal. Calorim.* **2021**, *144*, 1959–1983. [CrossRef]
17. Dubey, V.; Sharma, A.K. A short review on hybrid nanofluids in machining processes. *Adv. Mater. Process. Technol.* **2022**, 1–14. [CrossRef]
18. Ukueje, W.E.; Abam, F.I.; Obi, A. A perspective review on thermal conductivity of hybrid nanofluids and their application in automobile radiator cooling. *J. Nanotechnol.* **2022**, *2022*, 2187932. [CrossRef]
19. Harun, M.A.; Sidik, N.A.C.; Asako, Y.; Ken, T.L. Recent review on preparation method, mixing ratio, and heat transfer application using hybrid nanofluid. *J. Adv. Res. Fluid Mech. Therm. Sci.* **2022**, *95*, 44–53. [CrossRef]
20. Bachok, N.; Ishak, A.; Pop, I. Melting heat transfer in boundary layer stagnation-point flow towards a stretching/shrinking sheet. *Phys. Lett. A.* **2010**, *374*, 4075–4079. [CrossRef]
21. Bachok, N.; Ishak, A.; Pop, I. Mixed convection boundary layer flow over a moving vertical flat plate in an external fluid flow with viscous dissipation effect. *PLoS ONE* **2013**, *8*, e60766. [CrossRef] [PubMed]

22. Tadesse, F.B.; Makinde, O.D.; Enyadene, L.G. Mixed convection of a radiating magnetic nanofluid past a heated permeable stretching/shrinking sheet in a porous medium. *Math. Probl. Eng.* **2021**, *2021*, 6696748. [CrossRef]
23. Wahid, N.S.; Arifin, N.M.; Khashi'ie, N.S.; Pop, I.; Bachok, N.; Hafidzuddin, M.E.H. MHD mixed convection flow of a hybrid nanofluid past a permeable vertical flat plate with thermal radiation effect. *Alex. Eng. J.* **2022**, *61*, 3323–3333. [CrossRef]
24. Khan, M.R.; Pan, K.; Khan, A.U.; Nadeem, S. Dual solutions for mixed convection flow of SiO_2—Al_2O_3/water hybrid nanofluid near the stagnation point over a curved surface. *Phys. A Stat. Mech. Appl.* **2020**, *547*, 123959. [CrossRef]
25. Hanif, H.; Khan, I.; Shafie, S. Heat transfer exaggeration and entropy analysis in magneto-hybrid nanofluid flow over a vertical cone: A numerical study. *J. Therm. Anal. Calorim.* **2020**, *141*, 2001–2017. [CrossRef]
26. El-Zahar, E.R.; Rashad, A.M.; Saad, W.; Seddek, L.F. Magneto-hybrid nanofluids flow via mixed convection past a radiative circular cylinder. *Sci. Rep.* **2020**, *10*, 10494. [CrossRef]
27. Patil, P.M.; Kulkarni, M. Analysis of MHD mixed convection in a Ag-TiO_2 hybrid nanofluid flow past a slender cylinder. *Chin. J. Phys.* **2021**, *73*, 406–419. [CrossRef]
28. Abbasi, A.; Farooq, W.; Mabood, F. Mixed convective flow and heat transfer of hybrid nanofluid impinging obliquely on a vertical cylinder. *Int. J. Ambient. Energy* **2021**, *43*, 4343–4355. [CrossRef]
29. Jahan, S.; Ferdows, M.; Shamshuddin, M.; Zaimi, K. Radiative mixed convection flow over a moving needle saturated with non-isothermal hybrid nanofluid. *J. Adv. Res. Fluid Mech. Therm. Sci.* **2021**, *88*, 81–93. [CrossRef]
30. Patil, P.M.; Kulkarni, M. Effects of surface roughness and thermal radiation on mixed convective (GO–MoS2/H2O–C2H6O2) hybrid nanofluid flow past a permeable cone. *Indian J. Phys.* **2022**, *96*, 3567–3578. [CrossRef]
31. Asghar, A.; Ying, T.Y.; Zaimi, W.M.K.A.W. Two-dimensional mixed convection and radiative Al_2O_3-Cu/H_2O hybrid nanofluid flow over a vertical exponentially shrinking sheet with partial slip conditions. *CFD Lett.* **2022**, *14*, 22–38. [CrossRef]
32. Abdelaziz, A.H.; El-Maghlany, W.M.; El-Din, A.A.; Alnakeeb, M.A. Mixed convection heat transfer utilizing nanofluids, ionic nanofluids, and hybrid nanofluids in a horizontal tube. *Alex. Eng. J.* **2022**, *61*, 9495–9508. [CrossRef]
33. Khan, U.; Waini, I.; Zaib, A.; Ishak, A.; Pop, I. MHD mixed convection hybrid nanofluids flow over a permeable moving inclined flat plate in the presence of thermophoretic and radiative heat flux effects. *Mathematics* **2022**, *10*, 1164. [CrossRef]
34. Khan, U.; Zaib, A.; Ishak, A.; Sherif, E.M.; Waini, I.; Chu, Y.M.; Pop, I. Radiative mixed convective flow induced by hybrid nanofluid over a porous vertical cylinder in a porous media with irregular heat sink/source. *Case Stud. Therm. Eng.* **2022**, *30*, 101711. [CrossRef]
35. Gohar, T.S.K.; Khan, I.; Gul, T.; Bilal, M. Mixed convection and thermally radiative hybrid nanofluid flow over a curved surface. *Adv. Mech. Eng.* **2022**, *14*, 16878132221082848. [CrossRef]
36. Ahmed, S.E.; Raizah, Z.A. Magnetic mixed convection of a Casson hybrid nanofluid due to split lid driven heat generated porous triangular containers with elliptic obstacles. *J. Magn. Magn. Mater.* **2022**, *559*, 169549. [CrossRef]
37. Asghar, A.; Ying, T.Y.; Zaimi, K. Two-dimensional magnetized mixed convection hybrid nanofluid over a vertical exponentially shrinking sheet by thermal radiation, joule heating, velocity and thermal slip conditions. *J. Adv. Res. Fluid Mech. Therm. Sci.* **2022**, *95*, 159–179. [CrossRef]
38. Wafa, C.; Toufik, B. Mixed convection of hybrid nanofluid in inclined annulus subjected to solar radiation. *J. Thermophys. Heat Transf.* **2022**, *36*, 707–719. [CrossRef]
39. Mandal, D.K.; Biswas, N.; Manna, N.K.; Gorla, R.S.R.; Chamkha, A.J. Hybrid Nanofluid Magnetohydrodynamic Mixed Convection in a Novel W-Shaped Porous System. *Int. J. Numer. Methods Heat Fluid Flow*, 2022; *ahead-of-print*.
40. Gailitis, A.; Lielausis, O. On a possibility to reduce the hydrodynamic resistance of a plate in an electrolyte. *Appl. Magnetohydrodyn. Rep. Phys. Inst. Riga* **1961**, *12*, 143–146.
41. Magyari, E.; Pantokratoras, A. Aiding and opposing mixed convection flows over the Riga-plate. *Commun. Nonlinear Sci. Numer. Simul.* **2011**, *16*, 3158–3167. [CrossRef]
42. Pantokratoras, A.; Magyari, E. EMHD free-convection boundary-layer flow from a Riga-plate. *J. Eng. Math.* **2009**, *64*, 303–315. [CrossRef]
43. Bhatti, M.M.; Abbas, T.; Rashidi, M.M. Effects of thermal radiation and electromagnetohydrodynamics on viscous nanofluid through a Riga plate. *Multidiscip. Model. Mater. Struct.* **2016**, *12*, 605–618. [CrossRef]
44. Khatun, S.; Islam, M.M.; Mollah, M.; Poddar, S.; Alam, M. EMHD radiating fluid flow along a vertical Riga plate with suction in a rotating system. *SN Appl. Sci.* **2021**, *3*, 452. [CrossRef]
45. Grinberg, E. On determination of properties of some potential fields. *Appl. Magnetohydrodyn. Rep. Phys. Inst. Riga* **1961**, *12*, 147–154.
46. Ayub, M.; Abbas, T.; Bhatti, M.M. Inspiration of slip effects on electromagnetohydrodynamics (EMHD) nanofluid flow through a horizontal Riga plate. *Eur. Phys. J. Plus* **2016**, *131*, 193. [CrossRef]
47. Ahmad, R.; Mustafa, M.; Turkyilmazoglu, M. Buoyancy effects on nanofluid flow past a convectively heated vertical Riga-plate: A numerical study. *Int. J. Heat Mass Transf.* **2017**, *111*, 827–835. [CrossRef]
48. Goldstein, J. On backward boundary layers and flow in converging passages. *J. Fluid Mech.* **1965**, *21*, 33–45. [CrossRef]
49. Khashi'ie, N.S.; Arifin, N.M.; Pop, I. Mixed convective stagnation point flow towards a vertical Riga plate in hybrid Cu-Al_2O_3/water nanofluid. *Mathematics* **2020**, *8*, 912. [CrossRef]
50. Zainal, N.A.; Nazar, R.; Naganthran, K.; Pop, I. Unsteady stagnation point flow past a permeable stretching/shrinking Riga plate in Al_2O_3-Cu/H_2O hybrid nanofluid with thermal radiation. *Int. J. Numer. Methods Heat Fluid Flow* **2022**, *32*, 2640–2658. [CrossRef]

51. Wahid, N.S.; Arifin, N.M.; Khashi'ie, N.S.; Pop, I.; Bachok, N.; Hafidzuddin, M.E.H. Hybrid nanofluid stagnation point flow past a slip shrinking Riga plate. *Chin. J. Phys.* **2022**, *78*, 180–193. [CrossRef]
52. Alshehri, A.M.; Coban, H.H.; Ahmad, S.; Khan, U.; Alghamdi, W.M. Buoyancy effect on a micropolar fluid flow past a vertical Riga surface comprising water-based SWCNT–MWCNT hybrid nanofluid subject to partially slipped and thermal stratification: Cattaneo–Christov model. *Math. Probl. Eng.* **2021**, *2021*, 6618395. [CrossRef]
53. Khashi'ie, N.S.; Arifin, N.M.; Pop, I.; Wahid, N.S. Effect of suction on the stagnation point flow of hybrid nanofluid toward a permeable and vertical Riga plate. *Heat Transf.* **2021**, *50*, 1895–1910. [CrossRef]
54. Nadeem, S.; Ahmad, S.; Khan, M.N. Mixed convection flow of hybrid nanoparticle along a Riga surface with Thomson and Troian slip condition. *J. Therm. Anal. Calorim.* **2021**, *143*, 2099–2109. [CrossRef]
55. Nayak, M.K.; Mehmood, R.; Muhammad, T.; Khan, A.U.; Waqas, H. Entropy minimization in mixed convective Falkner-Skan flow of ZnO-SAE50 nanolubricant over stationary/moving Riga plate. *Case Stud. Therm. Eng.* **2021**, *26*, 101176. [CrossRef]
56. Ramzan, M.; Javed, M.; Rehman, S.; Ahmed, D.; Saeed, A.; Kumam, P. Computational assessment of microrotation and buoyancy effects on the stagnation point flow of Carreau–Yasuda hybrid nanofluid with chemical reaction past a convectively heated Riga plate. *ACS Omega* **2022**, *7*, 30297–30312. [CrossRef]
57. Salawu, S.O.; Obalalu, A.M.; Okoya, S.S. Thermal convection and solar radiation of electromagnetic actuator Cu-Al_2O_3/$C_3H_8O_2$ and Cu-$C_3H_8O_2$ hybrid nanofluids for solar collector optimization. *Mater. Today Commun.* **2022**, *33*, 104763. [CrossRef]
58. Shatnawi, T.A.M.; Abbas, N.; Shatanawi, W. Mathematical analysis of unsteady stagnation point flow of radiative Casson hybrid nanofluid flow over a vertical Riga sheet. *Mathematics* **2015**, *10*, 3573. [CrossRef]
59. Fang, T.; Zhang, J.; Zhong, Y. Note on unsteady viscous flow on the outside of an expanding or contracting cylinder. *Commun. Nonlinear Sci. Numer. Simul.* **2012**, *17*, 3124–3128. [CrossRef]
60. Rosseland, S. *Theoretical Astrophysics*; Clarendon Press: Oxford, UK, 1936.
61. Devi, S.U.S.; Devi, S.P.A. Heat transfer enhancement of Cu-Al_2O_3/water hybrid nanofluid flow over a stretching sheet. *J. Niger. Math. Soc.* **2017**, *36*, 419–433.
62. Takabi, B.; Salehi, S. Augmentation of the heat transfer performance of a sinusoidal corrugated enclosure by employing hybrid nanofluid. *Adv. Mech. Eng.* **2014**, *6*, 147059. [CrossRef]
63. Ahmed, N.; Tassaddiq, A.; Alabdan, R.; Adnan; Khan, U.; Noor, S.; Mohyud-Din, S.T.; Khan, I. Applications of nanofluids for the thermal enhancement in radiative and dissipative flow over a wedge. *Appl. Sci.* **2019**, *9*, 1976. [CrossRef]
64. Jafar, K.; Ishak, A.; Nazar, R. Magnetohydrodynamic stagnation point flow with a convective surface boundary condition. *Z. Für Nat. A* **2011**, *66*, 495–499. [CrossRef]
65. Mohamed, M.K.A.; Salleh, M.Z.; Nazar, R.; Ishak, A. Numerical investigation of stagnation point flow over a stretching sheet with convective boundary conditions. *Bound. Value Probl.* **2013**, *2013*, 4. [CrossRef]
66. Merkin, J.H. On dual solutions occurring in mixed convection in a porous medium. *J. Eng. Math.* **1986**, *20*, 171–179. [CrossRef]
67. Weidman, P.D.; Kubitschek, D.G.; Davis, A.M.J. The effect of transpiration on self-similar boundary layer flow over moving surfaces. *Int. J. Eng. Sci.* **2006**, *44*, 730–737. [CrossRef]
68. Harris, S.D.; Ingham, D.B.; Pop, I. Mixed convection boundary-layer flow near the stagnation point on a vertical surface in a porous medium: Brinkman model with slip. *Transp. Porous. Med.* **2009**, *77*, 267–285. [CrossRef]
69. Yahaya, R.I.; Arifin, N.M.; Ali, F.M.; Isa, S.S.P.M. Nanoparticle shapes effects on MHD flow of hybrid nanofluid over a stretching/shrinking sheet with slip and chemical reaction. *J. Nano Res.* **2022**, *75*, 139–158. [CrossRef]
70. Kierzenka, J. Tutorial on Solving BVPs with BVP4C. 2022. Available online: https://www.mathworks.com/matlabcentral/fileexchange/3819-tutorial-on-solving-bvps-with-bvp4c (accessed on 28 November 2022).
71. Ibrahim, W.; Anbessa, T. Mixed convection flow of nanofluid with Hall and ion-slip effects using spectral relaxation method. *J. Egypt Math. Soc.* **2019**, *27*, 52. [CrossRef]
72. Ganesh, N.V.; Al-Mdallal, Q.M.; Al Fahel, S.; Dadoa, S. Riga–Plate flow of γ Al_2O_3-water/ethylene glycol with effective Prandtl number impacts. *Heliyon* **2019**, *5*, e01651. [CrossRef]
73. Nayak, M.K.; Shaw, S.; Makinde, O.D.; Chamkha, A.J. Effects of homogenous–heterogeneous reactions on radiative NaCl-CNP nanofluid flow past a convectively heated vertical Riga plate. *J. Nanofluids* **2018**, *7*, 657–667. [CrossRef]